

Theoretical Study of Oxidative Additions of H₂ and MeCN to a Nickel(0) Complex: Significantly Large Correlation Effects and Characteristic Features of the Reaction

Yu-ya Ohnishi,[†] Yoshihide Nakao,[†] Hirofumi Sato,[†] and Shigeyoshi Sakaki^{*,‡}

Department of Molecular Engineering, Graduate School of Engineering, Kyoto University, Nishikyo-ku, Kyoto 615-8510, Japan, and Fukui Institute for Fundamental Chemistry, Kyoto University, Nishihiraki-cho, Takano, Sakyo-ku, Kyoto 606-8103, Japan

Received: March 6, 2007; In Final Form: May 22, 2007

Oxidative addition of H₂ to Ni(PH₃)₂ was theoretically studied as a prototype of nickel-catalyzed σ -bond activation reaction, where CASSCF, CASPT2, CCSD(T), broken symmetry (Bs) MP2 to MP4(SDTQ), and DFT methods were employed. The CASPT2 method yields a reliable potential energy curve (PEC) when the active space consists of 10 electrons and 10 orbitals including five outer 3d' orbitals. The CCSD(T) method presents almost the same PEC as the CASPT2-calculated one, when either the ANO or the cc-pVTZ basis set is used for Ni. Bs-MP4(SDTQ)-calculated PEC is similar to those calculated by the CASPT2/ANO method, while the PEC is not smooth around the transition state. In the DFT calculation, ANO, cc-pVTZ, and triple- ζ quality basis sets (SDB) with Stuttgart–Dresden–Bonn effective core potentials (ECPs) must be used for Ni. The DFT-calculated reaction energy is somewhat smaller than the CASPT2- and CCSD(T)-calculated values, while B3PW91 and mPW1PW91 present moderately better energy changes than BLYP, B1LYP, and B3LYP. Oxidative addition of MeCN to Ni(PH₃)₂ was investigated by the DFT(B3PW91) and CCSD(T) methods. Almost the same activation barrier was calculated by these methods, when cc-pVTZ was employed for Ni. However, the DFT method moderately underestimates the binding energy of the reactant complex and the reaction energy compared to the CCSD(T) method. This oxidative addition exhibits interesting characteristic features, as follows: The barrier height relative to infinite separation is lower, and the product is more stable than those of the oxidative addition of C₂H₆. These differences are discussed in detail in terms of Ni–Me and Ni–CN bond energies and the participation of the CN π^* orbital to stabilization interaction in the transition state.

1. Introduction

Activation of the C–CN σ -bond of nitrile by a low-valent transition-metal complex is one of the challenging reactions in organometallic chemistry, because it is not easy to activate the strong C–CN σ -bond with transition-metal complexes and the C–CN σ -bond activation can be utilized for organic synthesis. As a result of various attempts, several examples of stoichiometric C–CN σ -bond activation reaction by a transition-metal complex have been reported, so far: Previously, σ -bond activation of benzonitrile (PhCN) was succeeded with platinum(0),^{1,2} palladium(0),² and nickel(0)² complexes. Also, C–CN σ -bond activation with nickel(0)^{3,4} and molybdenum(0) complexes⁵ has been reported. Recently, the C–CN σ -bond activation by nickel(0) complexes was comprehensively investigated by Jones and his collaborators.⁶ Though these C–CN σ -bond activation reactions take place through the oxidative addition, a different type of C–CN σ -bond activation was performed with the help of the silyl group in rhodium(III)⁷ and iron(II) complexes.⁸ Besides these stoichiometric reactions, the C–CN σ -bond activation is included as a key elementary step in interesting catalytic reactions, Ni(0)-catalyzed biaryl synthesis⁹ and Ni(0)-catalyzed carbocyanation of alkyne.¹⁰

Considering that nickel(0) complexes have been often used in these stoichiometric and catalytic reactions, it is worth

investigating theoretically the C–CN σ -bond activation by nickel(0) complexes. However, no theoretical study has been reported about the C–CN σ -bond activation, and no detailed knowledge has been presented about it; for instance, knowledge of transition state structure and electronic process has not been reported yet, though it is necessary to understand well the C–CN σ -bond activation and catalytic reaction via the C–CN σ -bond activation.

As well-known, nondynamical (static) and dynamical electron correlation effects¹¹ must be carefully considered in the theoretical study of nickel complexes, actually, an outer (second) 3d' shell, which has one nodal plane in a radial part like a 4d shell, must be included in the active space of the CASPT2 calculation of Ni to present correct energy differences among various electronic states,¹² and incorporation of a 3p-3d intershell correlation is necessary for the evaluation of energy differences among various electronic states in the first-row transition-metal atoms.¹³ These results suggest to us to employ properly an active space in the multireference calculation. Also, many theoretical works have been carried out to evaluate binding energies of nickel(0) complexes with post Hartree–Fock^{12–28} and DFT^{29–32} methods. However, no organometallic reaction of a nickel complex has been theoretically investigated with a multireference method such as CASPT2 and MRMP2 methods, except for a few limited works;³³ in these pioneering works, the reaction of H₂ with a bare Ni atom was theoretically investigated with the CASSCF method, while the active space employed did not

* Corresponding author e-mail: sakaki@moleng.kyoto-u.ac.jp.

[†] Graduate School of Engineering.

[‡] Fukui Institute for Fundamental Chemistry.

include the outer 3d' shell. The lack of a multireference calculation of a chemical reaction is easily understood, as follows: Though active space should be adequately selected to incorporate well nondynamical correlation effects, such a selection cannot be easily made in the case of a reaction because orbital energy and orbital nature significantly change in the reaction in general.

Because of the above-mentioned difficulties in the theoretical study of nickel complexes, it is necessary to clarify what type of computational method should be applied to organometallic reactions of nickel complexes. In this work, we theoretically investigated the oxidative addition of H₂ to Ni(PH₃)₂. We selected this reaction as a prototype of Ni(0)-promoted σ -bond activation. Our purposes here are to clarify how much nondynamic and dynamic correlation effects are important in this type of reaction, what computational method should be applied, and what basis sets should be employed. Then, we theoretically investigated the C–CN σ -bond activation of MeCN by Ni(PH₃)₂ with the computational method that provides reliable results about the oxidative addition of H₂ to Ni(PH₃)₂. Our purposes of this part are to clarify the characteristic features of this C–CN σ -bond activation reaction and to present a detailed understanding of this reaction.

2. Computational Method

In the oxidative addition reaction of H₂ with Ni(PH₃)₂, reactant, transition state, and product were optimized by the DFT method with the B3LYP functional,^{34,35} where the Wachters basis set (14s9p5d1f)/[9s5p3d1f]³⁶ augmented with an f polarization function,³⁷ which is called Wa-TZ(f) hereafter, was used for Ni and 6-31G(d,p) basis sets³⁸ were employed for the other atoms. In all the stationary points, frequency calculations were performed to confirm if it was equilibrium structure or transition state. We also carried out an IRC calculation to ascertain if the transition state was connected with the reactant and the product.

Potential energy curves (PECs) were calculated by various methods and various basis sets, as follows: In CASSCF and CASPT2 calculations, the (21s15p10d6f)/[6s5p4d2f] basis set,³⁹ which is called ANO hereafter, was employed for Ni. In CCSD(T), broken-symmetry (Bs) MP2 to MP4(SDTQ),⁴⁰ and DFT calculations, ANO, cc-pVTZ,⁴¹ Wa-TZ(f),^{36,37} 6-31G(f),⁴² and m6-31G(f)⁴³ were employed for Ni, where one g-polarization function was omitted in the cc-pVTZ basis set. These all-electron basis sets are constructed for nonrelativistic calculations. Besides, the (311111/22111/411/1) basis set⁴⁴ was employed for valence electrons of Ni, and energy-consistent effective core potentials (ECPs) of the Stuttgart–Dresden–Bonn group were employed to replace its core electrons (up to 2p). This basis set is called SDB. Also, (761/681/51/1) and (7511/6711/411/1) basis sets⁴⁵ were employed for valence electrons of Ni, and the shape-consistent ECPs of Christiansen, Ermler, and co-workers⁴⁵ were employed to replace its core electrons. These basis sets are called CE-DZ and CE-TZ, respectively. These basis sets with ECPs include a relativistic effect in their potentials. BLYP,^{34,35} B1LYP,⁴⁶ B3PW91,⁴⁷ PBE1PBE,⁴⁸ and mPW1PW91⁴⁹ functionals were employed in DFT calculations. Bs-MP2 to Bs-MP4 methods were also used,⁴⁰ where the cc-pVTZ basis set was employed for Ni. In all these calculations, cc-pVDZ basis sets were employed for the other atoms. In several CCSD(T) calculations, we used cc-pVTZ basis sets⁵⁰ for ligand atoms to examine how much basis sets of ligand moiety influence computational results.

In the CASSCF calculations, three kinds of active space, (4e 4a), (10e 10a), and (12e 12a), were employed, where (*m na*)

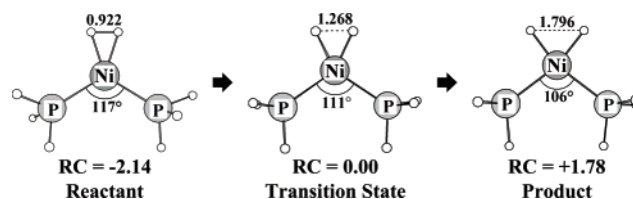


Figure 1. Geometry change in the oxidative addition of H₂ to Ni(PH₃)₂ optimized by the DFT(B3LYP) method. [The Wa-TZ(f) and 6-31G(d,p) basis sets were employed for Ni and the other atoms, respectively. All geometries have C₂ symmetry.] Bond lengths are in angstroms and bond angles are in degrees. RC means the reaction coordinate obtained by IRC calculation.

represents that the active space consists of *m* electrons and *n* orbitals. These active spaces will be discussed below in detail.

In the oxidative addition reaction of MeCN, all geometries were optimized by the DFT method with either B3LYP or B3PW91 functional, where Wa-TZ(f), SDB, and cc-pVTZ basis sets were employed for Ni and 6-31G(d,p) basis sets for the other atoms. In all the stationary points, frequency calculations were performed to confirm if it was equilibrium structure or transition state. To estimate an energy change, the CCSD(T) and DFT methods were employed where Wa-TZ(f), SDB, and cc-pVTZ basis sets were used for Ni and cc-pVDZ basis sets for the other atoms.

We used the Gaussian 03 program package⁵¹ for DFT, Bs-MP2 to MP4(SDTQ), and CCSD(T) calculations, and the MOLCAS (version 5.4) program package⁵² for CASSCF and CASPT2 calculations. Molecular orbitals were drawn with the MOLEKEL program.⁵³ Population analysis was carried out with the method of Weinhold et al.⁵⁴

3. Results and Discussion

3.1. Geometry Changes by Oxidative Additions of H₂ and MeCN to Ni(PH₃)₂. Geometry changes in the oxidative addition of H₂ to Ni(PH₃)₂ are shown in Figure 1, where RC represents the reaction coordinate evaluated by IRC calculation with the DFT(B3LYP) method. Although the product, *cis*-Ni(H)₂(PH₃)₂, could be optimized by the DFT(B3LYP)/Wa-TZ(f) method, the product became less stable than the transition state when a better basis set was employed, as will be discussed below in detail.

In the oxidative addition of MeCN, we investigated the basis set effects on geometries, where we concentrated on the transition state because the transition state structure significantly depends on the basis set in the oxidative addition of H₂ to Ni(PH₃)₂. We employed here Wa-TZ(f), cc-pVDZ, and SDB basis sets on Ni and 6-31G(d) on the other atoms; we will show that the quality of the cc-pVTZ is enough to present reliable energy changes below. The DFT(B3LYP)/Wa-TZ(f)-optimized transition state structure is considerably different from the DFT-(B3LYP)/cc-pVTZ- and DFT(B3LYP)/SDB-optimized ones; for example, the C–CN bond length is calculated to be 1.754 Å by the DFT(B3LYP)/Wa-TZ(f) method but 1.818 Å by the DFT-(B3LYP)/cc-pVTZ method (see Supporting Information Figure S1). On the other hand, the DFT(B3LYP)/SDB method provides almost the same transition state structure as the DFT(B3LYP)/cc-pVTZ-optimized one. These results indicate that Wa-TZ(f) cannot be used for Ni. Considering the large size of cc-pVTZ, we employed the SDB basis set for Ni in geometry optimization of the oxidative addition of MeCN to Ni(PH₃)₂ hereafter.

Then we optimized geometries of the reactant complex Ni(PH₃)₂(MeCN) **1a–1c**, transition state **TS**_{1–2}, and product *cis*-Ni(CN)(Me)(PH₃)₂ **2** with the DFT(B3LYP) and DFT(B3PW91) methods, as shown in Figures 2 and 10. Though both of these

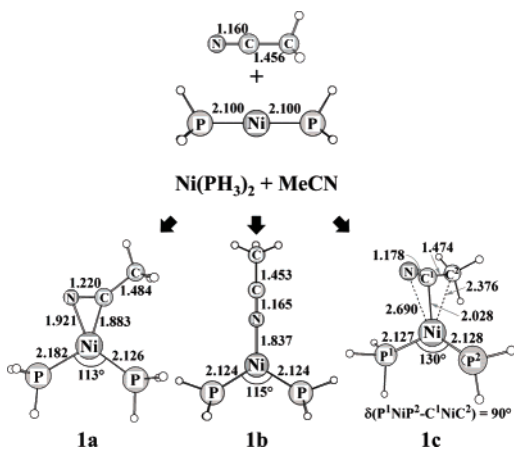


Figure 2. Three possible geometries of Ni(PH₃)₂(MeCN) optimized by the DFT(B3PW91) method. [SDB and 6-31G(d,p) basis sets were employed for Ni and the other atoms, respectively.] Bond lengths are in angstroms and bond angles are in degrees.

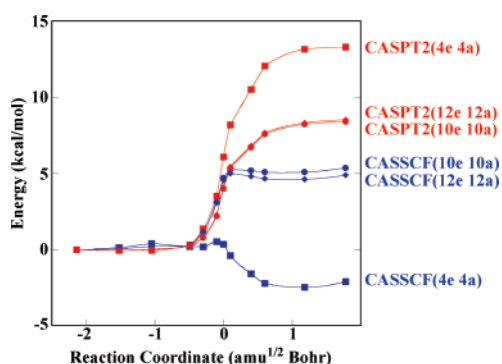


Figure 3. Potential energy curves of the oxidative addition of H₂ to Ni(PH₃)₂ calculated by the CASSCF and CASPT2 methods with the various active spaces. ANO and cc-pVDZ basis sets were employed for Ni and the other atoms, respectively.

two methods yield similar geometries of reactant, transition state, and product, the DFT(B3LYP) method failed to optimize one of the reactant complexes **1c** in which the C atom of the CN group interacts with the Ni center (see Supporting Information Figure S2 for the DFT(B3LYP)-optimized geometry changes). This is easily understood in terms of the fact that the C atom of CN weakly interacts with Ni(PH₃)₂ in **1c**, and the B3LYP functional is not useful very much for such a weak interaction; note that the B3PW91 functional is better than the B3LYP functional for van der Waals interaction.⁵⁵ It is concluded here that the DFT(B3PW91)/SDB method should be used for geometry optimization.

3.2. Energy Changes by Oxidative Additions of H₂ and MeCN to Ni(PH₃)₂. To investigate what computational method and basis sets present a reliable potential energy curve (PEC), we evaluated the energy changes by the oxidative addition of H₂ to Ni(PH₃)₂ with such computational methods as CASSCF, CASPT2, CCSD(T), Bs-MP2 to Bs-MP4(SDTQ), and DFT methods and various basis sets for Ni, where the DFT(B3LYP)/Wa-TZ(f)-optimized geometries were employed (see Figure 1). The CASSCF(4e 4a) method presents the downhill PEC, as shown in Figure 3. The (4e 4a) active space consists of occupied Ni(d), Ni(d) + H(1s), unoccupied Ni(d), and Ni(d)-H(1s) orbitals, as shown in Figure 4, where “+” and “−” represent bonding and antibonding combinations, respectively. The Ni-(d_σ) + H₂(σ) combination is observed in a canonical orbital, as shown in Figure 4. Although we included this orbital in the (4e 4a) active space, it changed to the Ni(d) orbital during CASSCF

calculation. This change suggests that intra 3d-shell correlation is important. It is noted that CASPT2 calculation with the same active space presents completely uphill PEC, which is totally different from the CASSCF(4e 4a) calculation. CASSCF(10e 10a) and CASSCF(12e 12a) calculations present uphill PEC, too, where the active space (10e 10a) consists of five occupied 3d orbitals and five second 3d' (outer 3d) orbitals, as shown in Figure 4. The active space (12e 12a) contains occupied 3p_z and unoccupied 4p_z orbitals in addition to 10 electrons and 10 orbitals of the (10e 10a) active space. We added these occupied 3p_z and unoccupied 4p_z orbitals to the active space, because the importance of 3p-3d correlation was reported previously.¹³ In this CASSCF(12e 12a) calculation, we included canonical MO-18a shown in Figure 4. However, this orbital changed to NO-15a during the CASSCF calculation. This means that the 3p-3d correlation is more important than the correlation arising from the dihydrogen σ orbital. The CASPT2(10e 10a) and CASPT2(12e 12a) calculations present more uphill PECs than those by CASSCF calculations with the same active spaces, indicating that dynamical correlation plays an important role in this reaction. Also, it is noted that (10e 10a) and (12e 12a) active spaces present almost the same PECs in both CASSCF and CASPT2 calculations. From these results, it should be concluded that (10e 10a) is necessary to incorporate well nondynamic correlation effects in this reaction but (4e 4a) is too small, the dynamical correlation plays an important role in this oxidative addition, and the CASPT2(10e 10a) method provides the reliable energy change of this oxidative addition reaction.

Then, we carried out CCSD(T), Bs-MP4, and DFT calculations, where the DFT(B3LYP)/Wa-TZ(f)-optimized geometries were employed (Figure 1). As shown in Figure 5, the endothermicity is calculated to be 7 kcal/mol by the CCSD(T)/ANO method. This is slightly smaller than the CASPT2(10e 10a)/ANO-calculated value by about 1.5 kcal/mol. To investigate basis set effects, cc-pVTZ, SDB, CE-TZ, CE-DZ, Wa-TZ(f), 6-31G(f), and m6-31G(f) were employed for Ni, where cc-pVDZ basis sets were employed for the other atoms. It is noted that the CCSD(T)/cc-pVTZ method presents almost the same PEC as that of the CCSD(T)/ANO method. When the other basis sets are employed for Ni, however, CCSD(T)-calculated PEC becomes completely different from the CASPT2(10e 10a)/ANO- and CCSD(T)/ANO-calculated ones. On the other hand, the CCSD(T)-calculated endothermicity depends slightly on the basis sets of ligand moiety; it is calculated to be 6.9 and 6.7 kcal/mol with cc-pVDZ and cc-pVTZ basis sets, respectively, where the cc-pVTZ basis set was employed for Ni. Here, we wish to mention the relativistic effect on the PEC. The Douglas–Kroll–Hess second-order scalar relativistic effect moderately decreases the endothermicity to 4.8 kcal/mol by about 2 kcal/mol in CCSD(T) calculation (see Supporting Information Figure S3). Also, it should be noted that the shape of PEC is still uphill and essentially the same as that by the nonrelativistic CCSD(T) calculation. This result indicates that the relativistic effect is not large in this system. We will present a discussion based on nonrelativistic calculations.

In Bs-MP2 to Bs-MP4(SDTQ) calculations, PEC considerably fluctuates, as shown in Figure 6; actually, the reaction is calculated to be exothermic by Bs-HF, Bs-MP2, Bs-MP3, Bs-MP4(D), and Bs-MP4(DQ) methods but endothermic by Bs-MP4(SDQ) and Bs-MP4(SDTQ) methods. The Bs-MP4(SDTQ) method yields almost the same endothermicity as that of the CASPT2(10e 10a)/ANO method. However, the Bs-MP4(SDTQ)-calculated PEC is not smooth around TS, though the fluctuation

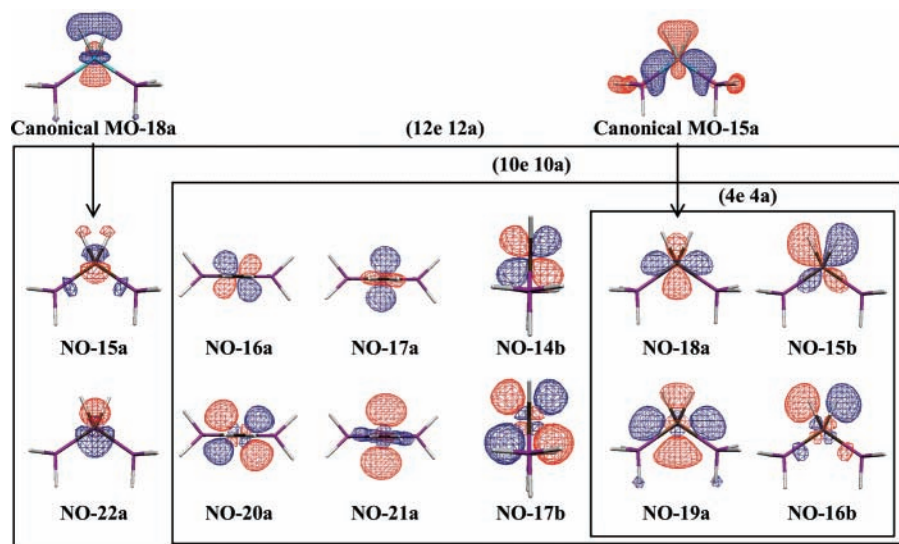


Figure 4. Pseudonatural orbitals (NOs) in the CASSCF calculations.

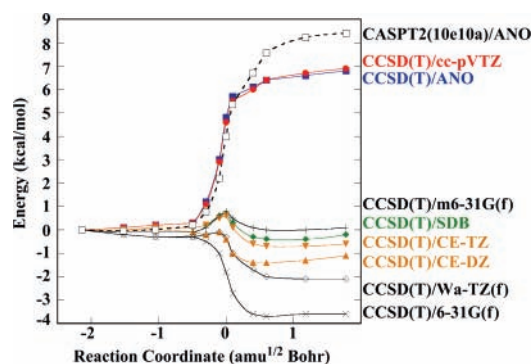


Figure 5. Potential energy curves of the oxidative addition of H_2 to $\text{Ni}(\text{PH}_3)_2$ calculated by the CCSD(T) method. Various basis sets were employed for Ni, and cc-pVDZ basis sets were employed for the other atoms.

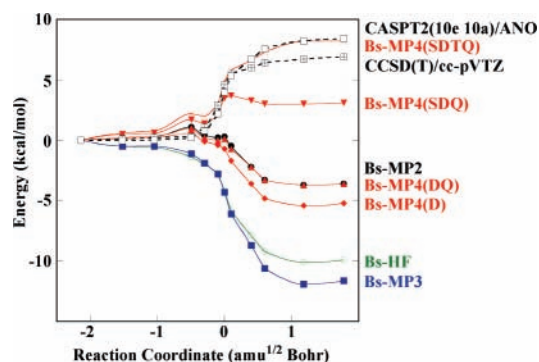


Figure 6. Potential energy curves of the oxidative addition of H_2 to $\text{Ni}(\text{PH}_3)_2$ calculated by the broken symmetry (Bs) MP2 to MP4(SDTQ) methods. The cc-pVTZ and cc-pVDZ basis sets were employed for Ni and the other atoms, respectively.

is small, being less than 0.5 kcal/mol. This nonsmooth PEC is interpreted in terms of fluctuation of singlet biradical nature;⁴⁰ the $\langle S^2 \rangle$ value of the Bs-HF wave function slightly increases from 0.5943 to 0.6064 upon going from RC = -2.14 to RC = -0.49 but then considerably decreases from 0.6064 to 0.3207 upon going from RC = -0.49 to RC = +1.78 (see Supporting Information Table S1). This change of $\langle S^2 \rangle$ value indicates that the singlet biradical nature slightly increases upon going from RC = -2.14 to RC = -0.49 but starts to decrease considerably after RC = -0.49. From these results, it is

concluded that the Bs-MP4(SDTQ) method should be applied carefully to this oxidative addition reaction, in particular, around TS.

In DFT calculations, basis set effects were first examined with the B3LYP functional, as shown in Figure 7(A). The DFT/ANO and DFT/cc-pVTZ methods yield uphill PEC like the CCSD(T)/ANO and CASPT2(10e 10a)/ANO methods, while the endothermicity is somewhat smaller than the CASPT2(10e 10a)/ANO- and CCSD(T)/ANO-calculated values. The DFT/SDB and DFT/CE-TZ methods present further smaller endothermicity than the DFT/ANO and DFT/cc-pVTZ methods, though the difference is small. DFT/m6-31G(f)- and DFT/CE-DZ-calculated PECs are still uphill but considerably different from CCSD(T)/cc-pVTZ- and DFT(B3LYP)/cc-pVTZ-calculated PECs. Both DFT/Wa-TZ(f) and DFT/6-31G(f) methods give completely different PECs from those of the CCSD(T)/ANO and CASPT2(10e 10a)/ANO methods. It is concluded that though basis set effects are not large in the DFT calculation in general, basis sets better than triple- ζ quality should be employed for Ni in this type of reaction.

Energy changes also somewhat depend on the functional, as shown in Figure 7(B). B3PW91, PBE1PBE, and mPW1PW91 present almost the same endothermicity, which is still smaller than those of the CCSD(T)/ANO and CASPT2(10e 10a)/ANO methods but moderately larger than those of B3LYP, BLYP, and B1LYP. Moreover, PECs calculated with B3PW91, PBE1PBE, and mPW1PW91 functionals are smooth, while those calculated with B3LYP, B1LYP, and BLYP are not.

We evaluated the energy changes of the oxidative addition of MeCN to $\text{Ni}(\text{PH}_3)_2$ with the CCSD(T)/cc-pVTZ method, because this method presents reliable energy changes in the oxidative addition of H_2 to $\text{Ni}(\text{PH}_3)_2$, where the DFT(B3PW91)/SDB-optimized geometries were employed. The activation barrier (E_a) is defined as an energy difference between TS_{1-2} and **1a** because **1a** is the most stable reactant complex. The reaction energy is defined as either an energy difference (ΔE_1) between the product **2** and the sum of reactant or the energy difference (ΔE_2) between **2** and the most stable reactant complex **1a**. As shown in Table 1, the E_a value is about 35 kcal/mol. This large E_a value indicates that this oxidative addition occurs with difficulty. The ΔE_1 value is -15.8 kcal/mol, but the ΔE_2 value is 14.7 kcal/mol; in other words, the product **2** is more stable than the sum of reactants but less stable than **1a**. These

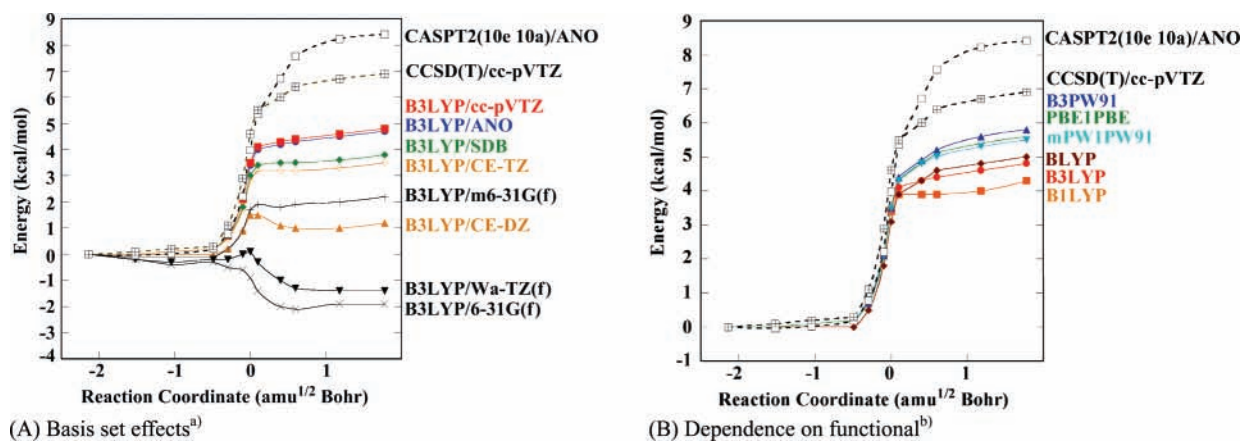


Figure 7. Potential energy curves of the oxidative addition of H₂ to Ni(PH₃)₂ calculated by the DFT method. a) Various basis sets were employed for Ni, and cc-pVTZ basis sets were employed for the other atoms. b) The cc-pVTZ and cc-pVDZ basis sets were employed for Ni and the other atoms, respectively.

TABLE 1: Energy Changes (kcal/mol) by the Oxidative Addition of MeCN to Ni(PH₃)₂

basis set for Ni	method	1a ^a	1b ^a	1c ^a	TS ₁₋₂ (E _a) ^b	2	
						ΔE ₁ ^c	ΔE ₂ ^d
cc-pVTZ	CCSD(T)	-30.5	-20.3	-7.1	5.4 (36.9)	-15.8	14.7
	DFT(B3PW91)	-26.4	-18.7	-3.0	10.7 (37.1)	-7.7	18.7
	DFT(B3LYP)	-22.0	-16.3	0.7	14.9 (36.9)	-5.7	16.3
SDB	CCSD(T)	-33.9	-18.9	-5.5	1.2 (35.1)	-25.5	8.4
	DFT(B3PW91)	-25.5	-17.6	-2.4	11.3 (36.8)	-7.6	17.9
	DFT(B3LYP)	-21.6	-15.4	1.4	15.1 (36.7)	-6.5	15.1
Wa-TZ(f)	CCSD(T)	-48.2	-27.7	-15.6	-16.5 (31.7)	-45.8	2.4
	DFT(B3PW91)	-43.0	-28.6	-13.8	-8.5 (34.5)	-32.1	10.9
	DFT(B3LYP)	-38.7	-26.2	-10.5	-4.4 (34.3)	-30.3	8.4

^a The energy difference between Ni(PH₃)₂(MeCN) and the sum of Ni(PH₃)₂ and MeCN. ^b The energy difference between TS₁₋₂ and 1a. ^c The energy difference between 2 and the sum of Ni(PH₃)₂ and MeCN. ^d The energy difference between 2 and 1a.

results indicate that the difficulty of this oxidative addition arises from the presence of too stable reactant complex 1a.

Also, we evaluated the energy changes with the CCSD(T), DFT(B3PW91), and DFT(B3LYP) methods with three basis sets for Ni to examine if the DFT method is useful or not in this reaction; note that it is important information as to how much the DFT-calculated energy deviates from that of the CCSD(T)/cc-pVTZ method because the CCSD(T)/cc-pVTZ method cannot be applied to the large system but the DFT/cc-pVTZ method can be applied. When cc-pVTZ and SDB are employed for Ni, the similar activation barrier (E_a) is evaluated by the CCSD(T), DFT(B3PW91), and DFT(B3LYP) methods, while the DFT method moderately underestimates the stability of 2. When the Wa-TZ(f) basis set is employed for Ni, all methods present considerably different energetics from the CCSD(T)/cc-pVTZ-calculated one; for example, the DFT(B3LYP)/Wa-TZ(f) and DFT(B3PW91)/Wa-TZ(f) methods give moderately different E_a values and considerably different ΔE₁ and ΔE₂ values from those of the CCSD(T)/cc-pVTZ method. These results show that Wa-TZ(f) cannot be used for these oxidative addition reactions of Ni(0) complex, as observed in the oxidative addition of H₂ to Ni(PH₃)₂.

These results lead to several important conclusions, as follows: (1) Either ANO or the cc-pVTZ basis set should be used for Ni in the CCSD(T) calculation, but SDB, CE-TZ, CE-DZ, Wa-TZ(f), 6-31G(f), and m6-31G(f) basis sets cannot be used. (2) The reliable energy changes are calculated with CASPT2(10e 10a)/ANO, CCSD(T)/ANO, and CCSD(T)/cc-pVTZ methods. (3) The Bs-MP4(SDTQ)/cc-pVTZ method should be used carefully around the transition state. (4) In the DFT calculation, ANO, cc-pVTZ, SDB, and CE-TZ should be used, while CE-DZ, m6-31G(f), Wa-TZ(f), and 6-31G(f) basis

sets cannot be used. (5) The DFT methods are useful to evaluate activation barrier. (6) We must be careful about the tendency of the DFT method to underestimate moderately the binding energy and the reaction energy.

3.3. Origin of Electron Correlation Effects. It is worth discussing the origin of the significantly large electron correlation effects in the oxidative addition of H₂ to Ni(PH₃)₂. We inspected the electron population of natural orbitals (NOs) evaluated by the CASSCF(10e 10a) method. As shown in Figure 8(A), the populations of NO-15b, NO-16b, NO-18a, and NO-19a considerably change, while the remains change slightly. This means that these four orbitals play a key role in the reaction. Consistent with these population changes, the weight of configuration 2 suddenly increases around TS but that of configuration 3 decreases around TS, as shown in Figure 8(B). Configuration 2 consists of two-electron excitation from NO-15b to NO-16b, where NO-15b and NO-16b mainly include Ni(d) + H(1s) bonding interaction and its antibonding counterpart, respectively. Thus, configuration 2 becomes important, when the Ni-H bond is formed. Configuration 3 mainly consists of one-electron excitation from NO-18a to NO-19a and that from NO-15b to NO-16b, where NO-18a and NO-19a mainly involve 3d and the outer (second) 3d' orbitals, respectively. Because the Ni-H bond is formed slightly before TS, this configuration corresponds not only to the correlation effect of the Ni-H bond but also to the intra 3d-shell correlation. In the CASSCF(4e 4a) calculation, these four orbitals are involved in the active space. However, the CASSCF(4e 4a)- and CASPT2(4e 4a)-calculated PECs are considerably different from the CASSCF(10e 10a)- and CASPT2(10e 10a)-calculated PECs, as discussed above. This significantly large difference indicates that the other type of electron correlation plays important roles. The (10e 10a)

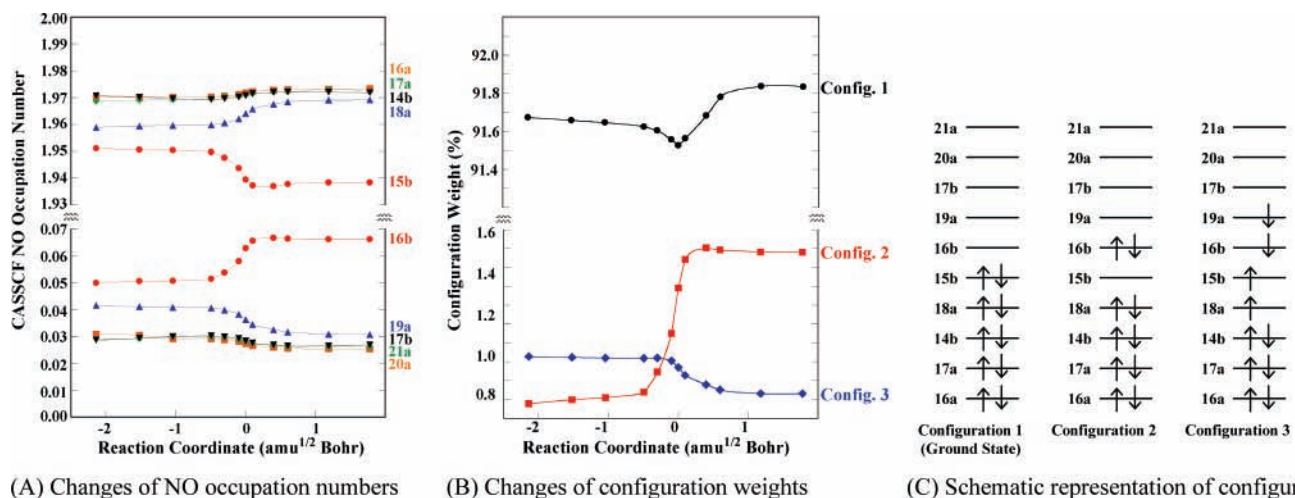


Figure 8. Occupation numbers of pseudonatural orbitals (NOs) and configuration weights in the oxidative addition of H₂ to Ni(PH₃)₂.

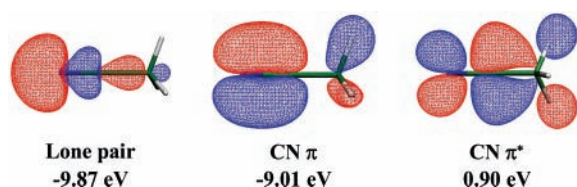
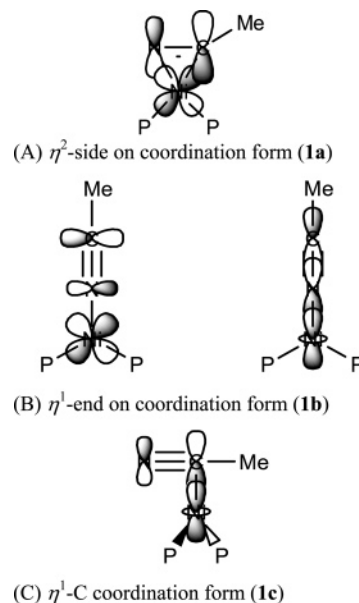


Figure 9. Three important molecular orbitals [Kohn–Sham orbital] of MeCN. The surface value is 0.05 au.

active space includes five doubly occupied 3d and the five outer (second) 3d' orbitals. These results suggest that incorporation of 3d' orbitals in active space is necessary to represent well 3d electron distributions because the outer 3d' orbitals have one nodal plane in the radial part, as shown in Figure 4. Note that the distributions and energies of 3d electrons are considerably changed by the oxidative addition reaction because the oxidation state of the metal center increases by 2 in a formal sense. This type of electron correlation effect is understood as “in–out” correlation.¹² In the first-row transition-metal complexes, this type of correlation is of particular importance, because the 3d orbitals are directly influenced by the change of the metal oxidation state due to the absence of the inner d shell.⁵⁶

3.4. Characteristic Feature of Oxidative Addition of MeCN to Ni(0) Complex. Here, we will discuss the characteristic features of the oxidative addition reaction of MeCN to Ni(PH₃)₂. In the reactant complex, three possible isomers were optimized, as already shown in Figure 2. In **1a**, the CN triple bond directly interacts with Ni. This η²-CN side-on coordination form is the most stable. The η¹-end-on coordination form **1b** is the next, and the η¹-C interacting form **1c** is the least stable. In **1a**, the C–N bond considerably lengthens to 1.220 Å. This is because MeCN coordinates to Ni mainly through the charge transfer from the Ni d_π orbital to the CN π* orbital; in other words, π-back-donation plays an important role. This π-back-donation is also responsible for the longer Ni–N distance than the Ni–C distance, as follows: The C p_π orbital contributes more to the CN π* orbital than to the N p_π orbital, as shown in Figure 9, which leads to larger overlap between Ni d_π and C p_π orbitals than that between Ni d_π and N p_π orbitals, as shown in Scheme 1A. In **1b**, the CN bond length (1.165 Å) is almost the same as that of free MeCN (1.160 Å). In this form, the π-back-donation somewhat participates in the coordinate bond, while its contribution is smaller than that in **1a** because the CN π* orbital overlaps less with the Ni d_π orbital than does the C p_π orbital due to the smaller contribution of the N p_π orbital than that of the C p_π orbital in the CN π* orbital, as shown in Scheme

SCHEME 1: Bonding Interaction between Ni(PH₃)₂ and MeCN



1b. The N lone pair orbital also participates in the coordinate bond through σ-donation (see also Scheme 1B). The π-back-donation leads to lengthening of the CN bond, while the σ-donation leads to shortening of the CN bond.⁵⁷ As a result, the CN bond length changes slightly by the coordination. In **1c**, the C atom of CN mainly interacts with Ni; actually, the Ni–N distance is considerably longer than the Ni–C distance. The CN (1.178 Å) bond is moderately longer than that of the free MeCN. This is easily interpreted in terms of the back-donation from the Ni d_σ to the CN π* orbital, as shown in Scheme 1C. This back-donation in **1c** is weaker than in **1a**, as follows: the Ni d_σ orbital interacts with the CN π* orbital more weakly than does the Ni d_π orbital, because the d_π orbital is HOMO and is at a higher energy than the d_σ orbital.^{58,59} The strength of back-donation can be also understood from the population changes of MeCN, as shown in Table 2. In **1a**, the population of MeCN considerably increases by the coordination, indicating that the considerably strong π-back-donation is formed between Ni and MeCN, as discussed above. The electron population of MeCN moderately increases in **1c** and the least in **1b**. These population changes are consistent with the above discussion that the π-back-donation mainly participates in the

TABLE 2: Population Changes^a by Coordination of MeCN with Ni(PH₃)₂

	1a	1b	1c
Ni	-0.4528	-0.3236	-0.2519
Ni(3d)	-0.2853	-0.1550	-0.0608
PH ₃ ¹	0.0137	0.1273	0.0565
PH ₃ ²	0.0150	0.1273	0.0565
MeCN	0.4241	0.0691	0.1389

^a A positive value means an increase in electron population and vice versa.

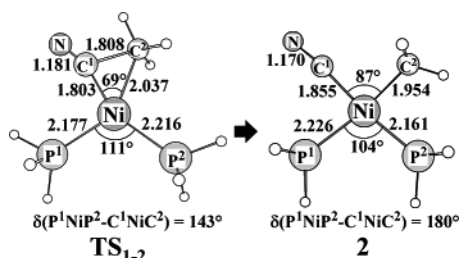


Figure 10. Geometry change in the oxidative addition of MeCN to Ni(PH₃)₂ optimized by the DFT(B3PW91) method, where SDB and 6-31G(d,p) basis sets were employed for Ni and the other atoms, respectively. Bond lengths are in angstroms and bond angles are in degrees.

coordinate bond of **1c**, but both the σ -donation and π -back-donation participate in the coordinate bond of **1b** to a similar extent.

In transition state **TS₁₋₂**, the C–CN bond considerably lengthens to 1.808 Å and the Ni–CN distance shortens to 1.803 Å, as shown in Figure 10, which is moderately shorter than that in the product, interestingly. It is also noted that the Ni–CH₃ distance is considerably longer than the Ni–CN distance. These geometrical features suggest that the Ni–CN bonding interaction induces the C–CN bond cleavage, which will be discussed below. It is also noted that the C–CN bond is not coplanar to the PNiP plane, but the dihedral angle between PNiP and CNiC planes is 143°. This type of nonplanar transition state structure was reported previously and analyzed in the oxidative additions of CH₃–CH₃ and CH₃–SiH₃ to Pt(PH₃)₂.⁶⁰ We omit the discussion of the nonplanar transition state structure here because detailed discussion was presented previously.⁶⁰

Product **2** is completely square planar. The Ni–P¹ bond is longer than the Ni–P² bond, indicating that the trans-influence effect of CH₃ is stronger than that of CN. This is because the Me group is electron-donating and the CN group is electron-withdrawing. We investigated the oxidative addition of ethane, C₂H₆, to Ni(PH₃)₂ to clarify the characteristic features of oxidative addition of MeCN to Ni(0) by making a comparison between C₂H₆ and MeCN. In this reaction, the reactant complex could not be optimized.⁶¹ In the transition state **TS₃₋₄**, the Ni–C distance is 1.942 Å, being moderately shorter than that of **TS₁₋₂** but somewhat longer than the Ni–CN distance of **TS₁₋₂**, as shown in Figure 11. The Ni–P distance is slightly longer than the Ni–P¹ distance of **TS₁₋₂** and moderately shorter than the Ni–P² distance of **TS₁₋₂**. This transition state is nonplanar, too, in which the dihedral angle is 114°. The product, *cis*-Ni(Me)₂(PH₃)₂ **4**, is a typical four-coordinate planar complex. The Ni–CH₃ distance is almost the same as that of **2**.

In the oxidative addition of C₂H₆ to Ni(PH₃)₂, **TS₃₋₄** and **4** are 25.2 (31.5) and 6.5 (13.8) kcal/mol less stable than the sum of reactants Ni(PH₃)₂ + C₂H₆, as shown in Figure 12, where the values without and with parentheses are CCSD(T)- and DFT-(B3PW91)-calculated values, respectively. This activation barrier is much smaller than that of the oxidative

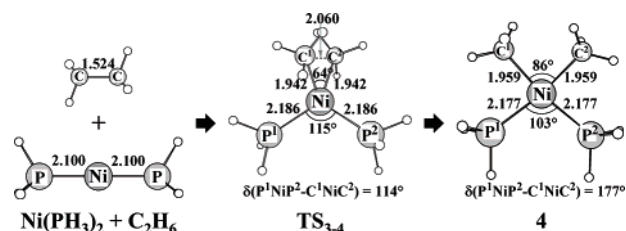


Figure 11. Geometry change in the oxidative addition of ethane to Ni(PH₃)₂ optimized by the DFT(B3PW91) method, where SDB and 6-31G(d,p) basis sets were employed for Ni and the other atoms, respectively. Bond lengths are in angstroms and bond angles are in degrees.

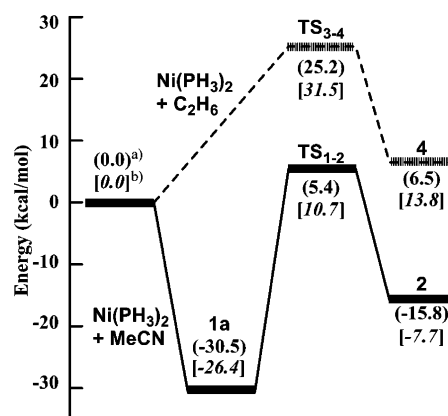


Figure 12. Energy changes (kcal/mol) in the oxidative addition of MeCN (solid line) and C₂H₆ (dashed line) to Ni(PH₃)₂. a) In parentheses are the CCSD(T)-calculated energy changes, where cc-pVTZ and cc-pVDZ basis sets were employed for Ni and the others, respectively. b) In brackets are the DFT(B3PW91)-calculated energy changes, where the same basis sets were employed as those of the CCSD(T)-calculation.

addition of MeCN to Ni(PH₃)₂. However, **TS₃₋₄** is much less stable than **TS₁₋₂**, if they are compared to the sum of reactants (see Figure 12). Thus, it is calculated that the smaller activation barrier of this oxidative addition arises from the absence of the stable reactant complex.

In these oxidative addition reactions, the charge-transfer (CT) interaction between the doubly occupied d_{π} orbital of Ni and the empty σ^* -antibonding orbital of MeCN and C₂H₆ plays important roles to break the C–C and C–CN σ -bond and to form M–Me and M–CN bonds.⁶² Such σ^* orbitals of MeCN and C₂H₆ are shown in Figure 13, where geometries are taken from the IRC calculations of oxidative additions of MeCN and C₂H₆. Apparently, LUMO is C–CN and C–C σ^* -antibonding orbitals in MeCN and C₂H₆, respectively, when the geometries of MeCN and C₂H₆ are taken to be the same as those of transition states. However, LUMO of free MeCN is the π^* orbital and that of free C₂H₆ is the C–H σ^* orbital. As shown in Scheme 2, the distortion of Me–CN induces the π^* - σ^* mixing, into which the π -bonding orbital mixes in an antibonding way with the σ^* -antibonding orbital because the π orbital is at lower energy than the σ^* orbital. These orbital mixings lead to the LUMO of distorted MeCN (Figure 13(A)). The distortion of C₂H₆ lowers the energy of the C–C σ^* -antibonding orbital because the antibonding overlap of orbitals decreases by the distortion, while the energy of the C–H σ^* -antibonding orbital changes slightly by the distortion. As a result, the C–C σ^* -antibonding orbital becomes LUMO in the distorted C₂H₆, and the C–H σ^* orbital becomes the next LUMO. It is noted that the LUMO of the distorted MeCN is at much lower energy than that of the distorted C₂H₆ (Figure 13). This is because the LUMO of MeCN mainly consists of the CN π^* orbital, which

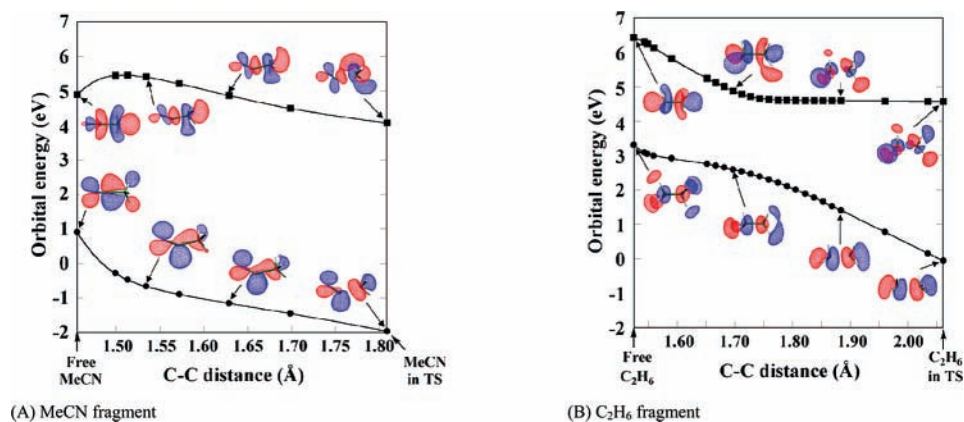
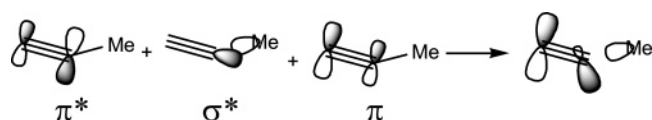


Figure 13. Two important unoccupied molecular orbitals [Kohn–Sham orbital] in (A) MeCN and (B) C₂H₆ fragments. Geometries of MeCN and C₂H₆ are taken from IRC calculations of the oxidative additions of MeCN and C₂H₆ to Ni(PH₃)₂.

SCHEME 2: Orbital Mixing in the CN π^* Orbital



is at much lower energy than the C–CN σ^* orbital, and the Me sp^3 orbital overlaps with the CN π^* orbital in a bonding way in the LUMO of distorted MeCN. As a result, the transition state of the C–CN σ -bond activation of MeCN is at lower energy than that of C₂H₆.

Differences in the electronic structure between the oxidative additions of MeCN and C₂H₆ to Ni(PH₃)₂ are found in the population changes, as shown in Figure 14. The electron populations of Me and CN groups considerably increase, and the Ni atomic population and the Ni d orbital population considerably decrease, as expected. These changes are consistent with our understanding that this is an oxidative addition reaction. It is noted that the sum of the electron population of Me and CN groups increases more in the oxidative addition of MeCN than in the sum of the electron population of two Me groups in the oxidative addition of C₂H₆. The Ni atomic population decreases more in the oxidative addition of MeCN than in the oxidative addition of C₂H₆. The significant difference is also observed in the population change of the PH₃ group: The population of PH₃ decreases more in the oxidative addition of MeCN than in the oxidative addition of C₂H₆. All these results arise from the following facts: the LUMO of MeCN is at a lower energy than that of C₂H₆, the CN group is electron-withdrawing, but the Me group is electron-donating.

Also, it is noted that **2** is more stable, but **4** is less stable than the sum of the reactants. To investigate these differences between MeCN and C₂H₆, we evaluated the Ni–Me and Ni–

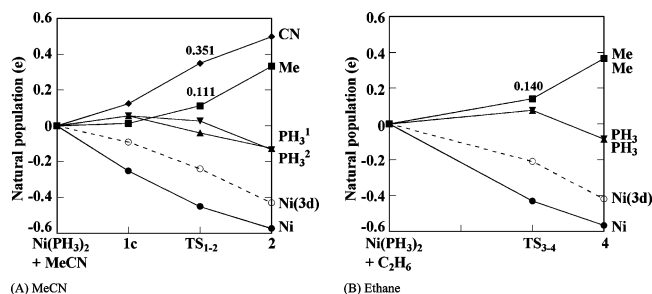
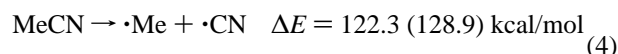
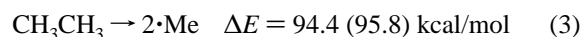
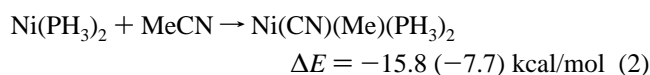
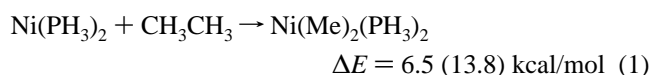


Figure 14. Changes of natural populations by oxidative additions of (A) MeCN and (B) ethane to Ni(PH₃)₂. The DFT(B3PW91) method was employed, where cc-pVTZ and cc-pVDZ basis sets were employed for Ni and the other atoms, respectively.

CN bond energies, considering the following reactions:



The difference in reaction energy between eqs 1 and 3 corresponds to twice the Ni–Me bond energy, and the reaction energy difference between eqs 2 and 4 corresponds to the sum of the Ni–Me and Ni–CN bond energies. Thus, the Ni–Me and Ni–CN bond energies are evaluated to be 44.0 (41.0) and 94.1 (95.7) kcal/mol, respectively. Though the C–CN bond of MeCN is considerably stronger than the C–C bond of C₂H₆ by 27.9 (33.1) kcal/mol, the Ni–CN bond is much stronger than the Ni–Me bond by 50.1 (54.7) kcal/mol. This is the reason why the oxidative addition of MeCN to Ni(PH₃)₂ is more exothermic than that of C₂H₆.

4. Conclusions

Oxidative addition of H₂ to Ni(PH₃)₂ was theoretically studied because this is considered as a prototype of a nickel-promoted σ -bond activation reaction. We employed here CASSCF, CASPT2, CCSD(T), broken symmetry (Bs) MP2 to MP4-(SDTQ), and DFT methods to investigate what methods present reliable results. In CASSCF and CASPT2 calculations, the active space should consist of 10 electrons and 10 orbitals which includes 3d and five outer 3d' orbitals. The CCSD(T) method presents almost the same result as the CASPT2 method with an active space of 10 electrons and 10 orbitals, when either the ANO or the cc-pVTZ basis set is used for Ni. However, the CCSD(T) method presents significantly different energy changes, when smaller basis sets than these two were employed for Ni. The Bs-MP4(SDTQ) method presents similar energy changes to those of the CCSD(T)/ANO, CCSD(T)/cc-pVTZ, and CASPT2/ANO methods, while the potential energy curve (PEC) is not smooth around the transition state. The DFT(B3LYP)-calculated reaction energy is somewhat smaller than the CASPT2- and CCSD(T)-calculated values, though the difference is not very large. ANO, cc-pVTZ, and triple- ζ quality basis sets with Stuttgart–Dresden–Bonn ECPs present much better results than the Wa-TZ(f) and 6-31G(f) basis sets in the DFT calculations.

B3PW91 and mPW1PW91 present moderately better energy changes than BLYP, B1LYP, and B3LYP.

Oxidative addition of MeCN to Ni(PH₃)₂ was investigated by the DFT(B3PW91) and CCSD(T) methods. These two methods present almost the same activation barrier, when cc-pVTZ is employed for Ni. However, the DFT method moderately underestimates the binding energy of the reactant complex and the reaction energy compared to the CCSD(T) method.

This oxidative addition exhibits interesting characteristic features, as follows: The barrier height is lower, and the product is more stable relative to infinite separation than those of the oxidative addition of C₂H₆. The lower barrier arises from the lower energy of the C–CN σ*-orbital of the distorted MeCN than that of the distorted C₂H₆. The larger exothermicity of the C–CN σ-bond activation arises from the stronger Ni–CN bond than the Ni–Me bond.

Acknowledgment. This work was financially supported by Grant-in-Aids on basic research (No. 15350012), Priority Areas for “Molecular Theory for Real Systems” (No. 461), Creative Scientific Research, and the NAREGI project from the Ministry of Education, Science, Sports, and Culture, and Research Fellowships of the Japan Society for the Promotion of Science for Young Scientists. Some of the theoretical calculations were performed with SX-7 workstations from the Institute for Molecular Science (Okazaki, Japan), and some of them were carried out with PC cluster computers from our laboratory.

Supporting Information Available: Complete form of refs 51 and 52, Cartesian coordinates of all species, DFT(B3LYP)-optimized geometries of Ni(PH₃)₂(MeCN) and Ni(CN)(Me)(PH₃)₂, and potential energy curves of the oxidative addition of H₂ to Ni(PH₃)₂ calculated by the nonrelativistic and relativistic CCSD(T) methods. This material is available free of charge via the Internet at <http://pubs.acs.org>.

References and Notes

- Gerlach, D. H.; Kane, A. R.; Parshall, G. W.; Jesson, J. P.; Muetterties, E. L. *J. Am. Chem. Soc.* **1971**, *93*, 3543.
- Parshall, G. W. *J. Am. Chem. Soc.* **1974**, *96*, 2360.
- (a) Morvillo, A.; Turco, A. *J. Organomet. Chem.* **1981**, *208*, 103. (b) Favero, G.; Morvillo, A.; Turco, A. *J. Organomet. Chem.* **1983**, *241*, 251.
- Abla, M.; Yamamoto, T. *J. Organomet. Chem.* **1997**, *532*, 267.
- Churchill, D.; Shin, J. H.; Hascall, T.; Hahn, J. M.; Bridgewater, B. M.; Parkin, G. *Organometallics* **1999**, *18*, 2403.
- (a) Garcia, J. J.; Jones, W. D. *Organometallics* **2000**, *19*, 5544. (b) Garcia, J. J.; Brunkan, N. M.; Jones, W. D. *J. Am. Chem. Soc.* **2002**, *124*, 9547. (c) Brunkan, N. M.; Brestensky, D. M.; Jones, W. D. *J. Am. Chem. Soc.* **2004**, *126*, 3627.
- (a) Taw, F. L.; White, P. S.; Bergman, R. G.; Brookhart, M. J. *Am. Chem. Soc.* **2002**, *124*, 4192. (b) Taw, F. L.; Mueller, A. H.; Bergman, R. G.; Brookhart, M. J. *Am. Chem. Soc.* **2003**, *125*, 9808.
- (a) Nakazawa, H.; Kawasaki, T.; Miyoshi, K.; Suresh, C. H.; Koga, N. *Organometallics* **2004**, *23*, 117. (b) Nakazawa, H.; Kamata, K.; Itazaki, M. *Chem. Commun.* **2005**, 4004.
- Miller, J. A. *Tetrahedron Lett.* **2001**, *42*, 6991.
- (a) Nakao, Y.; Oda, S.; Hiyama, T. *J. Am. Chem. Soc.* **2004**, *126*, 13904. (b) Nakao, Y.; Oda, S.; Yada, A.; Hiyama, T. *Tetrahedron* **2006**, *62*, 7567.
- (a) The nondynamical (static) correlation is understood in terms of the near degeneracy of several electronic states. The dynamical correlation is understood in terms of the electron correlation effects induced by collisions of two or more electrons. (b) Helgaker, T.; Jørgensen, P.; Olsen, J. *Molecular Electronic-Structure Theory*; John Wiley: New York, 2000.
- Andersson, K.; Roos, B. O. *Chem. Phys. Lett.* **1992**, *191*, 507.
- Pieloot, K.; Tsokos, E.; Roos, B. O. *Chem. Phys. Lett.* **1993**, *214*, 583.
- Bagus, P. S.; Roos, B. O. *J. Chem. Phys.* **1981**, *75*, 5961.
- (a) Walch, S. P.; Bauschlicher, C. W., Jr. *J. Chem. Phys.* **1983**, *78*, 4597. (b) Bauschlicher, C. W., Jr. *J. Chem. Phys.* **1986**, *84*, 260.

- Blomberg, M. R. A.; Brandemark, U. B.; Siegbahn, P. E. M.; Mathisen, K. B.; Karlström, G. *J. Phys. Chem.* **1985**, *89*, 2171.
- Widmark, P.-O.; Roos, B. O.; Siegbahn, P. E. M. *J. Phys. Chem.* **1985**, *89*, 2180.
- Bauschlicher, C. W., Jr.; Bagus, P. S.; Nelin, C. J.; Roos, B. O. *J. Chem. Phys.* **1986**, *85*, 354.
- Blomberg, M. R. A.; Brandemark, U. B.; Siegbahn, P. E. M.; Wennerberg, J.; Bauschlicher, C. W., Jr. *J. Am. Chem. Soc.* **2004**, *126*, 3627.
- Blomberg, M. R. A.; Brandemark, U. B.; Johansson, J.; Siegbahn, P.; Wennerberg, J. *J. Chem. Phys.* **1988**, *88*, 4324.
- Blomberg, M. R. A.; Siegbahn, P. E. M.; Lee, T. J.; Rendell, A. P.; Rice, J. E. *J. Chem. Phys.* **1991**, *95*, 5898.
- Sodupe, M.; Bauschlicher, C. W., Jr.; Lee, T. J. *Chem. Phys. Lett.* **1992**, *189*, 266.
- Pou-Américo, R.; Merchan, M.; Nebot-Gil, I.; Malmqvist, P.-A.; Roos, B. O. *J. Chem. Phys.* **1994**, *101*, 4893.
- Persson, B. J.; Roos, B. O.; Pierloot, K. *J. Chem. Phys.* **1994**, *101*, 6810.
- Pierloot, K.; Persson, B. J.; Roos, B. O. *J. Phys. Chem.* **1995**, *99*, 3465.
- Dapprich, S.; Ehlers, A. W.; Frenking, G. *Chem. Phys. Lett.* **1995**, *242*, 521.
- Bernardi, F.; Bottoni, A.; Calcinari, M.; Rossi, I.; Robb, M. A. *J. Phys. Chem. A* **1997**, *101*, 6310.
- Xu, X.; Lü, X.; Wang, N.; Zhang, Q.; Ehara, M.; Nakatsuji, H. *Int. J. Quantum Chem.* **1999**, *72*, 221.
- Jonas, V.; Thiel, W. *J. Chem. Phys.* **1995**, *102*, 8474.
- Adamo, C.; Lelj, F. *J. Chem. Phys.* **1995**, *103*, 10605.
- van Wüllen, C. *J. Chem. Phys.* **1996**, *105*, 5485.
- Hyla-Krypsin, I.; Koch, J.; Gleiter, R.; Klettke, T.; Walther, D. *Organometallics* **1998**, *17*, 4724.
- (a) Blomberg, M. R. A.; Siegbahn, P. E. M. *J. Chem. Phys.* **1983**, *78*, 986. (b) Blomberg, M. R. A.; Siegbahn, P. E. M. *J. Chem. Phys.* **1983**, *78*, 5682.
- (a) Becke, A. D. *Phys. Rev. A* **1988**, *38*, 3098. (b) Becke, A. D. *J. Chem. Phys.* **1993**, *98*, 5648.
- Lee, C.; Yang, W.; Parr, R. G. *Phys. Rev. B* **1988**, *37*, 785.
- Wachters, A. J. H. *J. Chem. Phys.* **1970**, *52*, 1033.
- Raghavachari, K.; Trucks, G. W. *J. Chem. Phys.* **1989**, *91*, 1062.
- (a) Hariharan, P. C.; Pople, J. A. *Theor. Chim. Acta* **1973**, *28*, 213. (b) Francl, M. M.; Pietro, W. J.; Hehre, W. J.; Binkley, J. S.; Gordon, M. S.; DeFrees, D. J.; Pople, J. A. *J. Chem. Phys.* **1982**, *77*, 3654.
- Pou-Américo, R.; Merchan, M.; Nebot-Gil, I.; Widmark, P.-O.; Roos, B. O. *Theor. Chim. Acta* **1995**, *91*, 149.
- (a) Čížek, J.; Paldus, J. *J. Chem. Phys.* **1967**, *47*, 3976. (b) Yamaguchi, K.; Fueno, T.; Fukutome, H. *Chem. Phys. Lett.* **1973**, *22*, 460. (c) Seeger, R.; Pople, J. A. *J. Chem. Phys.* **1977**, *66*, 3045. (d) Crawford, T. D.; Kraka, E.; Stanton, J. F.; Cremer, D. *J. Chem. Phys.* **2001**, *114*, 10638, and references therein.
- Balabanov, N. B.; Peterson, K. A. *J. Chem. Phys.* **2005**, *123*, 064107.
- Rassolov, V. A.; Pople, J. A.; Ratner, M. A.; Windus, T. L. *J. Chem. Phys.* **1998**, *109*, 1223.
- Mitin, A. V.; Baker, J.; Pulay, P. *J. Chem. Phys.* **2003**, *118*, 7775.
- Dolg, M.; Stoll, W. H.; Preuss, H. *J. Chem. Phys.* **1987**, *86*, 866.
- (a) Hurlley, M. M.; Fernandez Pacios, L.; Christiansen, P. A.; Ross, R. B.; Ermler, W. C. *J. Chem. Phys.* **1986**, *84*, 6840. (b) Couty, M.; Hall, M. B. *J. Comput. Chem.* **1996**, *17*, 1359. (c) Ehlers, A. W.; Böhme, M.; Dapprich, S.; Gobbi, A.; Höllwarth, A.; Jonas, V.; Köhler, K. F.; Stegmann, R.; Veldkamp, A.; Frenking, G. *Chem. Phys. Lett.* **1993**, *208*, 111.
- Adamo, C.; Barone, V. *Chem. Phys. Lett.* **1997**, *274*, 242.
- Perdew, J. P.; Wang, Y. *Phys. Rev. B* **1992**, *45*, 13244.
- Perdew, J. P.; Burke, K.; Ernzerhof, M. *Phys. Rev. Lett.* **1997**, *78*, 1396.
- Adamo, C.; Barone, J. *J. Chem. Phys.* **1998**, *108*, 664.
- Dunning, T. H., Jr. *J. Chem. Phys.* **1989**, *90*, 1007.
- Pople, J. A. et al. *Gaussian03, Revision C.02*; Gaussian, Inc.: Wallingford, CT, 2004.
- Widmark, P.-O. et al. *MOLCAS Version 5.4*; Lund University: Lund, Sweden, 2002.
- Flükiger, P.; Lüthi, H. P.; Portann, S.; Weber, J. *MOLEKEL v.4.3 for Scientific Computing*; Manno, Switzerland, 2002. Portman, S.; Lüthi, H. P. *Chimia* **2000**, *54*, 766.
- Reed, A. E.; Curtis, L. A.; Weinhold, F. *Chem. Rev.* **1988**, *88*, 849, and references therein.
- Tsuzuki, S.; Lüthi, H. P. *J. Chem. Phys.* **2001**, *114*, 3949.
- Frenking, G.; Fröhlich, N. *Chem. Rev.* **2000**, *100*, 717.
- The C–N distance of MeCN becomes shorter by interaction of MeCN with a proton; $R(\text{CN}) = 1.147 \text{ \AA}$ in $\text{MeCN} \cdots \text{H}^+$ and 1.160 \AA in free MeCN, where the DFT(B3PW91)/6-31G(d,p) method was used.

(58) (a) Albright, T. A.; Hoffmann, R.; Thibeault, J. C.; Thorn, D. L. *J. Am. Chem. Soc.* **1979**, *101*, 3801. (b) Sakaki, S.; Tsuru, N.; Ohkubo, K. *J. Phys. Chem.* **1980**, *84*, 3390.

(59) Similar differences in back-donation were reported in the η^2 -side on and the η^1 -C coordination CO₂ complexes of Ni(PH₃)₂.

(60) Sakaki, S.; Mizoe, N.; Musashi, Y.; Biswas, B.; Sugimoto, M. *J. Phys. Chem. A* **1998**, *102*, 8027.

(61) In the previous theoretical work with the MP2 method,⁵⁸ the reactant complex could be optimized. However, the stabilization energy is very small, indicating that the complex was in a very shallow minimum even if it was. Thus, the E_a value is influenced slightly by the presence of the reactant complex.

(62) Sakaki, S. *Top. Organomet. Chem.* **2005**, *12*, 31, and references therein.